Diagenetic priming of submarine landslides in ooze-rich substrates

Nan Wu[1*], Christopher A-L. Jackson [2], Michael A. Clare [3], David M. Hodgson [4], Harya D. Nugraha[5],

Michael J. Steventon[6], Guangfa Zhong[1]

[1]State Key Laboratory of Marine Geology, Tongji University, 1239 Siping Road, Shanghai, 200092, China

[2]Department of Earth and Environmental Sciences, University of Manchester, Oxford Road, Manchester, M13 9PL, UK

[3]National Oceanography Centre, Southampton SO14 3ZH, UK

[4]School of Earth and Environment, University of Leeds, Leeds, LS2 9JT, UK

[5]Center for Sustainable Geoscience, Universitas Pertamina, Jakarta, 12220, Indonesia

[6]Shell Research, Shell Centre, London, SE1 7NA, UK

Email: nanwu@tongji.edu.cn

Abstract

Oozes are the most widespread deep-sea sediment in the global ocean, but very little is known about how changes in their physical properties impact slope stability and related geohazards. Characterisation of the conditions that prime ooze rich slides has been hindered, as physical properties of sediments are modified by the effects of mass wasting. We here use 3D seismic reflection, geochemical, and petrophysical data acquired both within and adjacent to 13 large (up to c. 6330 km^2 in area) submarine slides on the Exmouth Plateau, NW Shelf, Australia, to investigate how the pre-slide physical properties of oozes control slope failure and slide emplacement. Our integrated dataset allows us to detect potential slide surfaces within ooze successions; a crucial advance for improved submarine geohazard assessment. Moreover, we demonstrate that the interplay of tectonics, ocean current activity, and silica diagenesis can prime multiple slides on very low gradient slopes in tropical, oceanic basins. We argue that the diagenesis of silica-rich sediments must be accounted for in future submarine slope stability assessments.

Keywords: Submarine landslides; Geohazard; Diagenesis; Oozes

Introduction

Submarine landslides (slides) can trigger tsunami and threaten coastal communities, and damage economically critically seabed infrastructure (e.g., Carter et al., 2012; Clare et al., 2014; Talling et al., 2014). It is now recognized that priming substrates to fail by post-depositional processes is a crucial control on their development and evolution, and that

instantaneous triggers, such as earthquakes, are not prerequisites for slide initiation (Masson et al., 2010; Talling et al., 2014; Urlaub et al., 2018). Such preconditioning appears to be particularly significant for calcareous oozes, with the biogenic constituents dominating such oozes having distinct geotechnical properties and failure behaviour, being highly compressible, water-rich, and prone to brittle inter-particle cementation. This potentially explains why large slides occur on unusually low-angle slopes (<2°) in areas of low sediment accumulation (<0.15 m/kyr) (e.g. Gatter et al., 2021; Urlaub et al., 2018). Despite their apparent significance, the pre-failure physical properties of ooze-rich slopes that ultimately fail remain poorly constrained (Urlaub et al., 2018), given: (i) difficulties in directly sampling and geophysically imaging the base of thick (100s m) slides; and (ii) slope failure modifies the slope's pre-failure physical properties.

Identifying potential failure or shear surfaces within sedimentary sequences is crucial for forecasting future events and modelling landslide motion (Locat et al., 2014). Previous studies have mostly focused on individual slides, specifically diatomaceous, rather than calcareous-ooze. Typically sampling has been from landslide debris; hence, any geotechnically-weak layers are unlikely to be preserved (Gatter et al., 2021; Locat et al., 2014; Urlaub et al., 2018). Therefore, the pre-emplacement physical properties of sediments at basal shear surfaces remain poorly understood, given they are likely strongly modified as the slide evolves (Masson et al., 2010). An understanding of the processes and timescales for priming calcareous ooze-rich slides is crucial to improve geohazard assessments, particularly given calcareous oozes are the most widespread deep-sea lithology (>50%; see Dutkiewicz et al., 2020).

We here integrate six time-migrated 3D seismic reflection datasets (16,189 km^2; see Appendix S1 for details), a regional network of 2D seismic reflection profiles, and lithological, petrophysical, and geochemical data from Ocean Drilling Program (ODP) site 762 on the Exmouth Plateau, NW Shelf, Australia (Figure 1A) to answer the following questions: i) what are the physical properties of calcareous ooze, and can they explain the stratigraphic occurrence of the basal shear surfaces of large slides? ii) to what extent does silica diagenesis modify subsurface physical properties, and prime substrate for sliding?, and iii) how important are regional tectonic and oceanographic controls in the preconditioning of calcareous-ooze slides?

Setting and Methods

Seismic reflection data image 13 slides that cumulatively cover c. 6330 km^2 within the Upper Miocene and Recent interval of the Exmouth Plateau (Horizon H2 to the seabed; Figure 1B), which is equivalent to Seismic Unit 3 of Nugraha et al. (2018). ODP 762 and industrial boreholes indicate this interval comprises calcareous oozes (Nugraha et al., 2018). ODP 762 is unaffected by sliding, but intersects an interval stratigraphically-equivalent to that hosting the slides, hence we are able to characterize the pre-failure stratigraphy (Figure 2A, 2B). We mapped three, age-constrained (see below) seismic horizons that define distinct changes in seismic facies and thus bound two seismic units (SU1-2): (i) H1 – intra-Upper Eocene; (ii) H2 – the Late Miocene Unconformity (Haq et al., 1990; Nugraha et al., 2018); and (iii) H3 – an undated horizon that defines the top surface of the largest slide (Slide-1; 2,800 km^2), which merges with H2 near the Exmouth Plateau Arch (Figure 1C). Variance attributes (see Appendix S2 for explanation) were generated to determine the extent and geometry of these seismic facies and inferred depositional bodies. Seismic reflection data were tied to petrophysical, lithological, and geochemical data from ODP 762, allowing us corelate seismic character and sediment properties (Haq et al., 1992; Scarselli et al., 2013). Velocity data from ODP 762 provide a proxy record of sediment overpressure (see method outlined by Dugan and Sheahan, 2012), whereas water content is used as a proxy for the sediment shear strength and compressibility (Urlaub et al., 2018).

Results

Horizon H1: Opal A-CT Conversion Boundary

Horizon H1 defines the base of SU1 (Figure 1C). It is offset by numerous, low-throw (<20 ms TWT) polygonal faults that terminate at, or just below, H2 (Figure 1B, 2C). Well-log data reveal a distinct change in petrophysical properties downwards across H1, defined by a sharp increase in bulk density (from 1.80 g/cm^3 to 2.17 g/cm^3) and velocity (from 1.62 km/s to 1.86 km/s), and a decrease in porosity (from 58.0% to 42.5%) and water content (from 30.0% to 20.7%) (Figure 1B). This dramatic downward change in physical properties is expressed in the seismic reflection data by a discrete, c. 40 ms TWT-thick package of high-amplitude reflections, broadly defined at its top by a positive polarity event (i.e., a downward increase in acoustic impedance; Figure 1B, 2C). X-ray diffraction measurements

94 (XRD) from ODP 762 also show that sediments above H1 have high concentrations of opal A,

95 whereas below H1, the sediment has high concentrations of opal CT (Figure 1B). H1

96 therefore corresponds to the opal A-CT conversion boundary (Haq et al., 1990; Nähr et al.,

97 1998).

98 *SU-1 - Lower Eocene to Upper Miocene chalk affected by silica diagenesis*

99 The basal part of SU-1 is enriched in clinoptilolite (Figure 1B), one of the most common

100 authigenic silicate minerals in pelagic sediments (Nähr et al., 1998). SU1 transitions upwards

101 from competent, hard chalk (Lower Eocene-Upper Eocene) to calcareous ooze (Upper

102 Eocene-Middle Miocene) (Figure 1B), and it is deformed by the polygonal fault system

103 offsetting H1 (Figure 1B, 2C). Data from ODP 762 show that the dissolved SiO_2 content

104 increases over a 50 m-thick interval near the top of SU-1 (Figure 1B). The dominant

105 diagenetic process associated with SU-1 is therefore interpreted to be silica diagenesis, with

106 the locally abundant clinoptilolite interpreted to be caused by the conversion of opal A to CT

107 (Volpi et al., 2003).

108 *Horizon H2 – Late Miocene Unconformity and regional failure plane for slides*

109 H2 defines the base of SU2 (Figure 2C and Appendix S3 for Slides 2-13). The bases of all 13

110 slides identified in this unit are on, or only 15-30 m above, H2. Well-log data from ODP 762

111 indicate H2 corresponds to a major, biostratigraphically-defined unconformity, separating

112 Late Eocene and Late Miocene deposits (Haq et al., 1990; Nugraha et al., 2018). H2 defines a

113 sharp upward increase in terrigenous particles (e.g. quartz, feldspar, and clay), and

114 nearshore coccolithophores (e.g. *Braarudosphaera Bigelow*), the latter being extremely

115 unusual for deep-marine basinal sediments, and providing possible evidence for an abrupt

116 change in the paleo-ocean current regime associated with Australia-Eurasia collision during

117 the Late Miocene (Haq et al., 1990).

118 Well-log data from ODP 762 also reveal a distinct change in petrophysical parameters across

119 H2, with bulk density increasing downward from 1.60 g/cm^3 to 1.85 g/cm^3, and porosity

120 decreasing downward from 80% to 58.5% (Figure 1B). The extremely low density and

121 velocity response below H2 indicates that abnormally high overpressure may have been

122 trapped below this horizon (Figure 1B; Dugan and Sheahan, 2012; Tingay et al., 2009).

123 Conversely, the locally low porosity response at the same level may indicate H2 is over-

124 compacted, with an extremely low permeability compared to the underlying sediment

125 (Figure 1B). It is these sharp changes in petrophysical properties that result in H2 being

126 expressed by a high-amplitude, negative polarity seismic reflection (Figure 1B). Another

127 petrophysically-distinct layer, Hs (c.10 m thick), immediately above H2 (Figure 1B), is

128 characterized by an upward decrease in Vp from 1.7 km/s and 1.52 km/s, and an increase in

129 water content from 30% to 48.5% (Figure 1B). The extremely low velocity response at the

130 level of Hs indicates possible underpressure at this horizon, whereas the high-water content

131 response indicates Hs has higher compressibility and lower shear strength.

132 *Seismic Unit 2: Slide-prone calcareous ooze interval affected by polygonal faulting and*

133 *dewatering*

134 SU2 contains pure calcareous ooze (Late Miocene-present) (Figure 1B) and is dominated by

135 chaotic seismic facies of highly variable amplitude. The exception to this being near ODP 762,

136 where continuous, low-amplitude reflections occur (Figure 1C). We interpret that the

137 chaotic and continuous seismic facies represent slide (e.g., Bull et al., 2009) and background

138 slope deposits, respectively. We now focus on Slide-1, the largest and best-imaged slide, to

139 investigate the role of substrate preconditioning and triggering of the slides on the Exmouth

140 Plateau (Figure 2A, 2B).

141 Below Slide-1, H1 is crosscut by numerous polygonal faults that tip-out upward at or near its

142 basal shear surface (i.e., H2; Figure 3A, 3B). H3 defines the top of Slide-1 and is a high-

143 amplitude, negative polarity reflection (Figure 3A). Directly beneath H2 are numerous high-

144 amplitude, wavy reflections that are developed close to the upper termination of the faults

145 (Figure 3A). In planform, these reflections define sub-circular (<100 m in diameter) to

146 elliptical (100-500 m long-axis length) depressions (Figure 3C), interpreted as sediment

147 accumulation (e.g. Paganoni et al., 2019). The high-amplitude wavy reflections resemble

148 zones of sediment accumulation due to fluid expulsion or gas migration as observed

149 elsewhere on the Exmouth Plateau (Foschi and Cartwright, 2020; Paganoni et al., 2019). The

150 spatial relationships between the sediment accumulation and the upper tips of polygonal

151 faults suggest the fluids driving the formation of the former migrated along the latter.

152 **Discussion and Conclusion**

153 *Controls on the formation of a regional failure surface and slide emplacement*

154 Compared with H2, the c. 10 m-thick Hs is characterized by relatively high-water content
155 (and hence low shear strength and high compressibility) and a low acoustic velocity, both
156 indicative of overpressure (Figure 4B). The geotechnical contrast between impermeable
157 strata underlying the regional H2 unconformity and the overlying water-saturated, over-
158 pressured ooze of SU2, created a weak layer, providing ideal conditions for slope failure,
159 even on very low angle slopes. We propose this explains why all thirteen slides share a
160 stratigraphically-equivalent failure surface, with Hs ultimately being locally entrained by the
161 slides.

162 A similar diagnosis was made in the shallower water Finneidfjord, Norway where multiple,
163 asynchronous fjord-flank slides share a regional failure plane, above which a low density,
164 over-pressured layer was deposited (L'Heureux et al., 2012). While the source of the weak
165 layer was terrestrially-derived mud and not deep water calcareous ooze, the similarity of a
166 highly compressible fluid-charged mud overlying an impermeable basal layer is striking.
167 Overpressure in Finneidfjord is related to the infiltration of meteoric groundwater. However,
168 such terrestrially-linked charging is not possible in the deep water setting of the Exmouth
169 Plateau, thus we discuss alternative mechanisms for overpressure development and
170 subsequent slope failure.

171 *Silica diagenesis as a primer for slope instability and failure, and slide emplacement*

172 We suggest that the most likely source for overpressure relates to the generation and
173 release of fluids during silica diagenesis, which is a well-known dehydration reaction (e.g.,
174 Davies et al., 2009; Volpi et al., 2003). The pronounced downward decrease in porosity and
175 water content below H1 suggests a large amount of fluid was expelled from the opal A-CT
176 conversion zone (Figure 4a, 4c; Davies and Clark, 2006). This fluid migrated upward, likely
177 along polygonal faults (e.g. Davies et al., 2009; Gay et al., 2006; Lüdmann et al., 2022) and
178 became trapped beneath the lower permeability Horizon H2, creating stratigraphically-
179 controlled overpressure and lowering the sediment shear strength (Figure 4B, C, D).
180 Whether such fluid migration is steady and continuous, or intermittent, perhaps triggered
181 by transient periods of seismicity, remains unclear (e.g. Embriaco et al., 2014). It is plausible
182 that enhanced seismicity, as a result of the Australian and Eurasian plates colliding during
183 the Early Miocene, could triggered fluid flow and maybe even slope failure (Nugraha et al.,
184 2018). Regardless, our findings support previous proposals of silica diagenesis priming

185   relatively local submarine slope instability and the emplacement of small, single slide (c. 110

186   km^2 in area; Davies and Clark, 2006; Volpi et al., 2003). Our study is the first to identify this

187   control in a tropical setting, and to show it can create a regional failure plane for multiple,

188   large volume submarine landslides.

189   *Role of tectonics and paleo-oceanography in priming and dictating the location of slope*

190   *failure*

191   During the Late Miocene, a global sea-level fall and the collision of the Australia and Eurasia

192   Plates caused the Indonesian ocean gateway to narrow offshore north Australia (Nugraha et

193   al., 2018). This caused an increase in the inflow of warm south Pacific waters, thus

194   increasing the strength of the southward flowing Leeuwin Current and suppressing the deep

195   northward-flowing Western Australia Current (Rai and Singh, 2001). These tectonically-

196   driven variations in ocean circulation fundamentally controlled the benthic and planktonic

197   foraminiferal assemblages (Srinivasan, 1985), and hence the abrupt contrast in lithology and

198   physical properties at H2 that subsequently primed submarine landslide failure depth and

199   location. The interplay of multiple physical processes on slide preconditioning can thus be

200   felt thousands, or even millions, of years after their activity has ceased (Gatter et al., 2020),

201   thus cautioning against the simplistic linkage of sliding to an external trigger. We suggest

202   that such a temporally-buffered connection likely exists for many other settings, where

203   diverse tectonic, sedimentological and/or oceanographic process interactions create

204   stratigraphically-constrained fluid sources, pathways, and permeability barriers (Gatter et al.,

205   2021; Gatter et al., 2020; L'Heureux et al., 2012).

206   **Figure Caption**

207   Figure 1. (A) Location of the study area. The red polygons and grey lines represent the 3D

208   and 2D seismic reflection data, respectively. Ocean current pathways are modified by

209   Nugraha et al. (2018). (B) Log-seismic integration at ODP 762. The lithology and age

210   correlation is interpreted from the ODP 762 scientific report (Haq et al., 1990). Direct

211   seismic to well ties between Bonaventure 3D and ODP 762 has been undertaken by Scarselli

212   et al. (2013). (C) Regional composite seismic section across the study area showing the main

213   tectonic elements and seismic units.

214　Figure 2. (A) The seabed time structure map shows the location of the thirteen slides that

215　have shaped the seabed of the study area. (B) Sketch of Figure 2A. (C) Seismic section across

216　Slide-1 shows the key seismic horizons and seismic units.

217　Figure 3. (A) Zoomed-in seismic section of Slide-1. (B) Variance time slice calculated c. 130 ms

218　below Slide-1, revealing polygonal fault systems. (C) Variance time slice calculated c. 40 ms

219　below Slide-1, showing pipe-like and crater-like structures. See the time slice location in

220　Figure 3A. See the location of Figure 3 in Figure 2B.

221　Figure 4. Schematic diagram showing the development of the slides. (A) Deposition of the

222　siliceous chalk stage. (B) Vp and water content curves at the ODP 762 reveal the potential

223　sliding surface (Hs). (C) Deposition of the calcareous oozes and opal A-CT (H1) conversion

224　stage. (D) Deposition of the regionally distributed slides stage.

229　**Reference**

230　Bull, S., Cartwright, J., and Huuse, M., 2009, A review of kinematic indicators from mass-transport
231　　　complexes using 3D seismic data: Marine and Petroleum Geology, v. 26, no. 7, p. 1132-1151.
232　Carter, L., Milliman, J., Talling, P., Gavey, R., and Wynn, R., 2012, Near‐synchronous and delayed
233　　　initiation of long run‐out submarine sediment flows from a record‐breaking river flood,
234　　　offshore Taiwan: Geophysical Research Letters, v. 39, no. 12, p. 1-5.
235　Clare, M. A., Talling, P. J., Challenor, P., Malgesini, G., and Hunt, J., 2014, Distal turbidites reveal a
236　　　common distribution for large (> 0.1 km3) submarine landslide recurrence: Geology, v. 42,
237　　　no. 3, p. 263-266.
238　Davies, R., Ireland, M., and Cartwright, J., 2009, Differential compaction due to the irregular topology
239　　　of a diagenetic reaction boundary: a new mechanism for the formation of polygonal faults:
240　　　Basin Research, v. 21, no. 3, p. 354-359.
241　Davies, R. J., and Clark, I. R., 2006, Submarine slope failure primed and triggered by silica and its
242　　　diagenesis: Basin Research, v. 18, no. 3, p. 339-350.
243　Dugan, B., and Sheahan, T., 2012, Offshore sediment overpressures of passive margins: Mechanisms,
244　　　measurement, and models: Reviews of Geophysics, v. 50, no. 3, p. 1-20.
245　Dutkiewicz, A., Judge, A., and Müller, R. D., 2020, Environmental predictors of deep-sea polymetallic
246　　　nodule occurrence in the global ocean: Geology, v. 48, no. 3, p. 293-297.
247　Embriaco, D., Marinaro, G., Frugoni, F., Monna, S., Etiope, G., Gasperini, L., Polonia, A., Del Bianco, F.,
248　　　Çağatay, M. N., and Ulgen, U. B., 2014, Monitoring of gas and seismic energy release by
249　　　multiparametric benthic observatory along the North Anatolian Fault in the Sea of Marmara
250　　　(NW Turkey): Geophysical Journal International, v. 196, no. 2, p. 850-866.
251　Foschi, M., and Cartwright, J., 2020, Seal failure assessment of a major gas field via integration of
252　　　seal properties and leakage phenomena: AAPG Bulletin, v. 104, no. 8, p. 1627-1648.

253   Gatter, R., Clare, M., Kuhlmann, J., and Huhn, K., 2021, Characterisation of weak layers, physical
254   controls on their global distribution and their role in submarine landslide formation: Earth-
255   Science Reviews, v. 223, p. 103845.

256   Gatter, R., Clare, M. A., Hunt, J. E., Watts, M., Madhusudhan, B., Talling, P. J., and Huhn, K., 2020, A
257   multi-disciplinary investigation of the AFEN Slide: the relationship between contourites and
258   submarine landslides: Geological Society, London, Special Publications, v. 500, no. 1, p. 173-
259   193.

260   Gay, A., Lopez, M., Cochonat, P., Séranne, M., Levaché, D., and Sermondadaz, G., 2006, Isolated
261   seafloor pockmarks linked to BSRs, fluid chimneys, polygonal faults and stacked Oligocene–
262   Miocene turbiditic palaeochannels in the Lower Congo Basin: Marine Geology, v. 226, no. 1-
263   2, p. 25-40.

264   Haq, B., Boyd, R., Exon, N., and Von Rad, U., Evolution of the central Exmouth Plateau: a post-drilling
265   perspective, in Proceedings Proceedings of the Ocean Drilling Program, Scientific
266   Results1992, Volume 122, ODP Ocean Drilling Program, p. 801-816.

267   Haq, B., von Rad, U., and Leg, O., 1990, 122 Shipboard Scientific Party, 1990: Proc. ODP, Ink. Repts, v.
268   122, p. 9-15.

269   L'Heureux, J.-S., Longva, O., Steiner, A., Hansen, L., Vardy, M. E., Vanneste, M., Haflidason, H.,
270   Brendryen, J., Kvalstad, T. J., and Forsberg, C. F., 2012, Identification of weak layers and their
271   role for the stability of slopes at Finneidfjord, northern Norway, Submarine mass
272   movements and their consequences, Springer, p. 321-330.

273   Locat, J., Leroueil, S., Locat, A., and Lee, H., 2014, Weak layers: their definition and classification
274   from a geotechnical perspective, Submarine mass movements and their consequences,
275   Springer, p. 3-12.

276   Lüdmann, T., Betzler, C., Lindhorst, S., Lahajnar, N., and Hübscher, C., 2022, Submarine landsliding in
277   carbonate ooze along low-angle slopes (Inner Sea, Maldives): Marine and Petroleum
278   Geology, v. 136, p. 105403.

279   Masson, D., Wynn, R., and Talling, P., 2010, Large landslides on passive continental margins:
280   processes, hypotheses and outstanding questions, Submarine mass movements and their
281   consequences, Springer, p. 153-165.

282   Nähr, T., Botz, R., Bohrmann, G., and Schmidt, M., 1998, Oxygen isotopic composition of low-
283   temperature authigenic clinoptilolite: Earth and Planetary Science Letters, v. 160, no. 3-4, p.
284   369-381.

285   Nugraha, H. D., Jackson, C. A. L., Johnson, H. D., Hodgson, D. M., and Reeve, M. T., 2018, Tectonic
286   and oceanographic process interactions archived in Late Cretaceous to Present deep‐
287   marine stratigraphy on the Exmouth Plateau, offshore NW Australia: Basin Research, v. 31,
288   no. 3, p. 405-430.

289   Paganoni, M., King, J. J., Foschi, M., Mellor-Jones, K., and Cartwright, J. A., 2019, A natural gas
290   hydrate system on the Exmouth Plateau (NW shelf of Australia) sourced by thermogenic
291   hydrocarbon leakage: Marine and Petroleum Geology, v. 99, p. 370-392.

292   Rai, A., and Singh, V., 2001, Late Neogene deep-sea benthic foraminifera at ODP Site 762B, eastern
293   Indian Ocean: diversity trends and palaeoceanography: Palaeogeography, Palaeoclimatology,
294   Palaeoecology, v. 173, no. 1-2, p. 1-8.

295   Scarselli, N., McClay, K., and Elders, C., 2013, Submarine slide and slump complexes, Exmouth
296   Plateau, NW Shelf of Australia, in Proceedings The Sedimentary Basins of Western Australia
297   IV: Proceedings of the Petroleum Exploration Society of Australia Symposium, Perth,
298   WA2013, Volume 18.

299   Srinivasan, K. J. K. G., 1985, Miocene planktonic foraminiferal biogeography and pale-oceanographic
300   development of the Indo-Pacific region: The Miocene Ocean: Paleoceanography and
301   biogeography: Boulder, Colorado Geologic Society of America Memoir, p. 197-236.

302   Talling, P. J., CLARE, M. L., Urlaub, M., Pope, E., Hunt, J. E., and Watt, S. F., 2014, Large submarine
303   landslides on continental slopes: geohazards, methane release, and climate change:
304   Oceanography, v. 27, no. 2, p. 32-45.
305   Tingay, M. R., Hillis, R. R., Swarbrick, R. E., Morley, C. K., and Damit, A. R., 2009, Origin of
306   overpressure and pore-pressure prediction in the Baram province, Brunei: Aapg Bulletin, v.
307   93, no. 1, p. 51-74.
308   Urlaub, M., Geersen, J., Krastel, S., and Schwenk, T., 2018, Diatom ooze: Crucial for the generation of
309   submarine mega-slides?: Geology, v. 46, no. 4, p. 331-334.
310   Volpi, V., Camerlenghi, A., Hillenbrand, C. D., Rebesco, M., and Ivaldi, R., 2003, Effects of biogenic
311   silica on sediment compaction and slope stability on the Pacific margin of the Antarctic
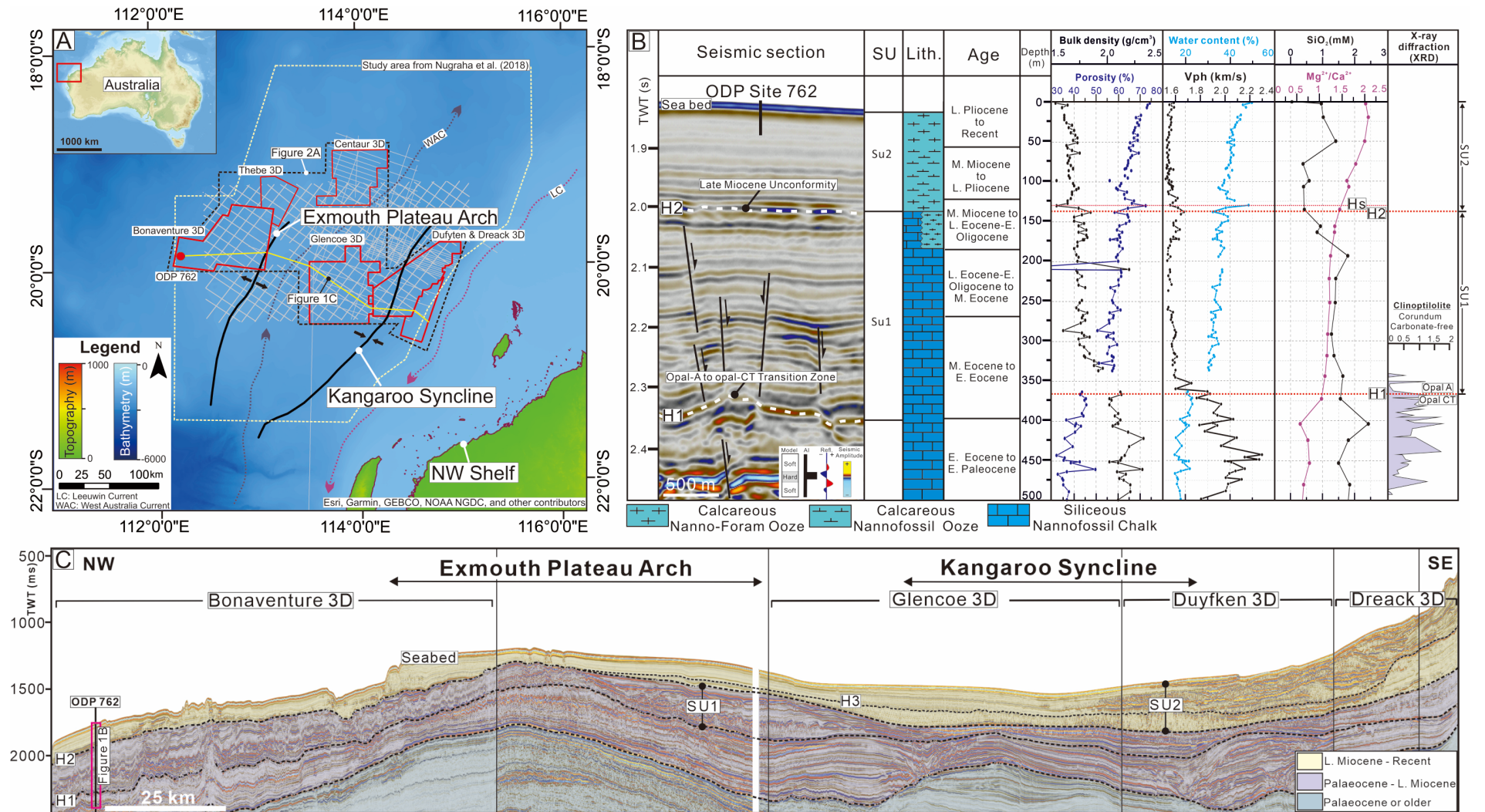312   Peninsula: Basin Research, v. 15, no. 3, p. 339-363.

Figure 1
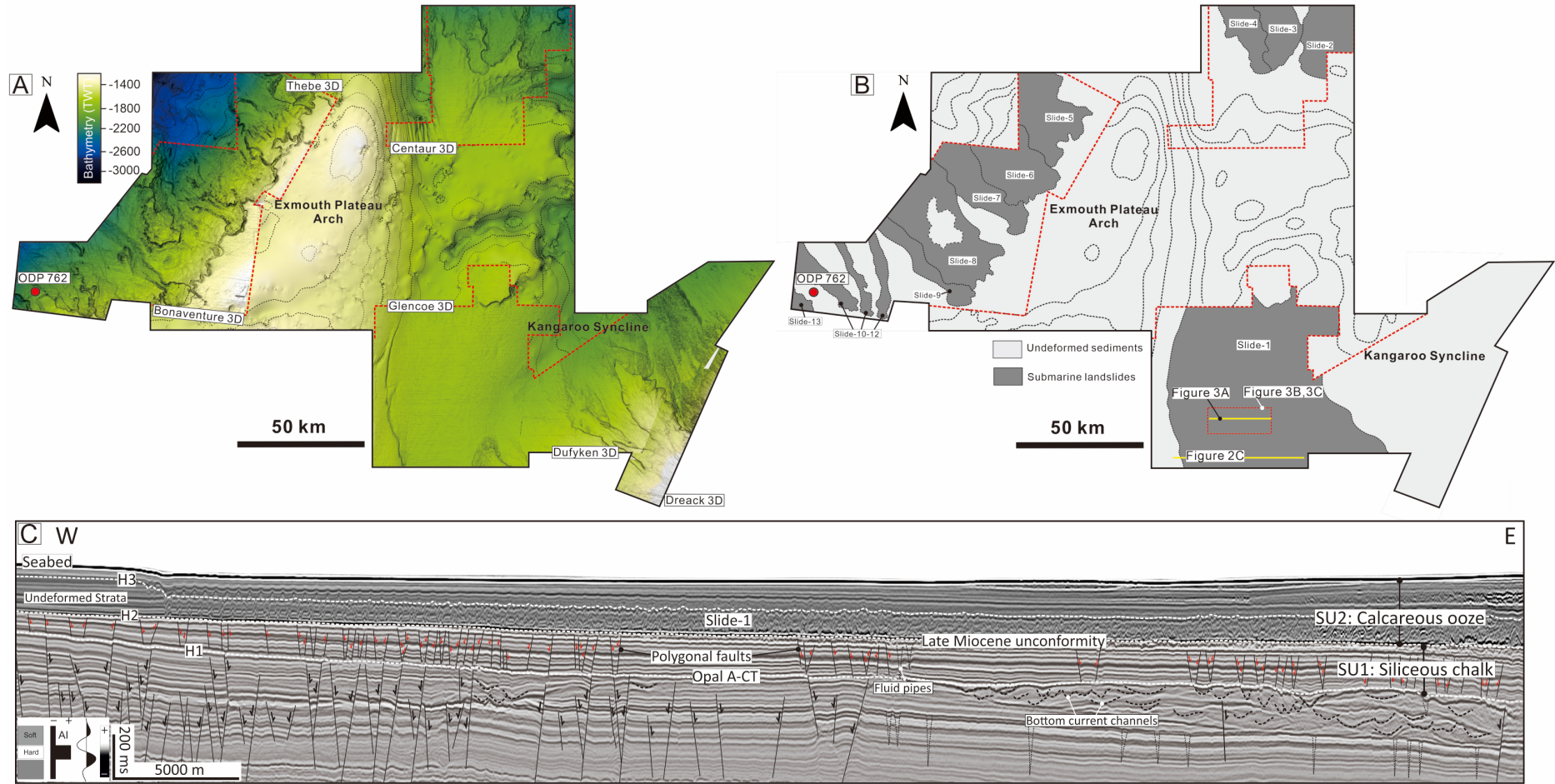

A — Map of study area offshore Western Australia showing Exmouth Plateau Arch, Kangaroo Syncline, NW Shelf, and 3D survey areas (Centaur 3D, Thebe 3D, Bonaventure 3D, Glencoe 3D, Dufyten & Dreack 3D), ODP 762, Figure 2A, Figure 1C. Legend: Topography (m), Bathymetry (m). LC: Leeuwin Current; WAC: West Australia Current. Study area from Nugraha et al. (2018). Esri, Garmin, GEBCO, NOAA NGDC, and other contributors.

B — Seismic section at ODP Site 762 with SU, Lith., Age, Bulk density (g/cm³), Water content (%), SiO₂ (mM), Porosity (%), Vph (km/s), Mg²⁺/Ca²⁺, and X-ray diffraction (XRD) logs. Features: Sea bed, Late Miocene Unconformity, H2, Opal-A to opal-CT Transition Zone, H1. Ages: L. Pliocene to Recent; M. Miocene to L. Pliocene; M. Miocene to L. Eocene-E. Oligocene; L. Eocene-E. Oligocene to M. Eocene; M. Eocene to E. Eocene; E. Eocene to E. Paleocene. Lithology: Calcareous Nanno-Foram Ooze; Calcareous Nannofossil Ooze; Siliceous Nannofossil Chalk. Model: Soft, Hard, Soft; AI; Refl.; Seismic + Amplitude. Clinoptilolite, Corundum, Carbonate-free. Opal A / Opal CT. Hs, H2, H1.

C — NW–SE seismic cross section (TWT ms) showing Bonaventure 3D, Exmouth Plateau Arch, Kangaroo Syncline, Glencoe 3D, Duyfken 3D, Dreack 3D. Labels: Seabed, ODP 762, Figure 1B, H2, H1, H3, SU1, SU2, 25 km scale. Legend: L. Miocene – Recent; Palaeocene – L. Miocene; Palaeocene or older.

Figure 2

Figure 3

A W ... E

Seabed
H3
Slide-1
H2
Figure 3C
H1
Figure 3B

SU-2
SU-1

Gas/Fluid accumulation
Polygonal faults

100 ms
500 m
Soft / Hard
AI

B 5 km
N
High
Low
Variance
Polygonal faults

C 5 km
N
High
Low
Variance
Gas/Fluid accumulation

Figure 4